Irradiation-driven evaporation of micro droplets in an optical trap

Jugal Shah [1], Max Huisman [2,*], Devendra Deshmukh [1], Dag Hanstorp [3] and Javier Tello Marmolejo [3,†]

[1] *Department of Mechanical Engineering, Indian Institute of Technology Indore, India*

[2] *SUPA and School of Physics and Astronomy, The University of Edinburgh, Peter Guthrie Tait Road, Edinburgh EH9 3FD, United Kingdom*

[3] *Department of Physics, University of Gothenburg, SE-412 96 Gothenburg, Sweden*

(Received 14 December 2024; accepted 30 April 2026; published 15 June 2026)

In many natural and industrial environments, small droplets are irradiated with visible and infrared light, affecting how they evaporate. Without external heating, droplets usually shrink faster as they become smaller. The simplest description of this is the D^2 law, where the shrinking rate dR/dt is proportional to $t^{-1/2}$ or R^{-1}. However, modeling this becomes more complicated when irradiation-driven volumetric heating is considered, and only few studies have investigated the evaporation behavior of levitating droplets under strong irradiation. Here we show the effects of weak and strong irradiation on single, optically levitated, micrometer-sized water droplets. We find that the droplets shrink following distinct accelerating and decelerating regimes, that we characterize through two power laws. Under weak irradiation, the shrinking rate accelerates, similar to the D^2 law. Under strong irradiation, however, the shrinking decelerates following the power law $dR/dt \sim R$, i.e., inverse of the D^2 law. Between these two regimes, at radii of 3–5 μm, a turnover occurs from decelerating shrinking back to accelerating shrinking. Our findings shed new light on droplet evaporation under weak and strong irradiative heating, such as mists under sunshine or fuel droplets irradiated by flames in rocket engines or internal combustion.

DOI: 10.1103/92w3-x9q4

I. INTRODUCTION

Evaporation of small liquid droplets into the surrounding gas phase is ubiquitous in nature and industry. In spray drying for pharmaceutical and medical applications, evaporation is used to produce fine particles [1,2]. In combustion science, understanding the evaporation of fuel droplets is essential for optimizing engine performance and fuel efficiency [3,4]. Other applications include cloud formation [5] and drug delivery through aerosols [6].

In many of these systems, droplets are subject not only to convective and diffusive processes but also to radiative heating, which significantly alters their evaporation dynamics. For example, in combustion chambers and rocket engines, fuel droplets are exposed to intense thermal radiation and flame fronts [7]; in atmospheric conditions, solar radiation affects aerosol-cloud interactions [8];

[*] Present address: Leiden Institute of Physics (LION), Leiden University, Niels Bohrweg 2, 2333 CA Leiden, The Netherlands.

[†] Contact author: javier.marmolejo@physics.gu.se

Published by the American Physical Society under the terms of the Creative Commons Attribution 4.0 International license. Further distribution of this work must maintain attribution to the author(s) and the published article's title, journal citation, and DOI. Funded by Bibsam.

and in diagnostic studies, laser-based techniques such as LIF (laser-induced fluorescence) [3] may unintentionally introduce thermal gradients within the droplets. Understanding how such radiative energy inputs influence evaporation of small droplets remains an open question.

To study the influence of irradiation on the evaporation of droplets suspended in air, we here consider techniques that minimize additional contributions to the evaporation dynamics, such as convective effects that are relevant for free-falling droplets [9] or surface-related evaporation effects that can be significant under IR heating [10]. Therefore, we focus on experimental techniques where levitating droplets can be fixed in position in the air. Examples of frequently used techniques include electrostatic [11] or acoustic traps [12]. However, electrostatic methods require charging the droplets, which can lead to charge saturation [13] and instability [14]. As the droplets evaporate, it can even lead to Coulomb explosions, limiting the minimum size of the droplets at radii of about 5 μm [15,16]. Furthermore, acoustic traps are suitable only for much larger droplets with minimum sizes of about 1 mm [17] due to their low inertia and the large wavelength of the sound used to trap.

Optical trapping, particularly using a counter-propagating configuration [18], enables the study of small droplets, where radii from 1 μm to 10 μm can be accurately measured, which is not possible in many other experimental techniques. These traps provide precise and contact-free confinement of small droplets, and have been used to study evaporation rates [19], refractive index measurements [20], Raman spectroscopy [21], and water uptake in organic aerosols [22]. Another advantage of using optical traps is that by varying the laser intensity, the power available for radiative heating can be adjusted [23].

Here, we investigate the evaporation dynamics of individual, optically levitated water droplets as they shrink from 10 to 1 μm in radius under weak and intense irradiative heating.

We compare our experimental results to the D^2 law, which describes the quasisteady evaporation of a spherical droplet into a gaseous medium. It predicts that the surface area of the droplet decreases linearly with time [24], leading to an accelerating shrinking rate following the power law $\dot{R}(t) \sim R^{-1}$. We will call $\dot{R}(t)$ the "shrinking rate" and not "evaporation rate" since the latter is commonly used to describe the change of mass as a function of time, instead of the change in radius. For weak irradiative heating, we observe accelerating shrinking rates, representing only a small deviation from the D^2 law.

However, under strong irradiative heating, we show that the evaporation greatly deviates from the classical D^2 law behavior: the shrinking rate of droplets decelerates instead of accelerating. In this regime, the evaporation is driven by the irradiative heating and can be described by a simple power law where the shrinking rate decreases linearly with the radius, i.e., $\dot{R}(t) \sim R$. This behavior is very different from predictions using numerical methods [25,26], where only a slight deviation from the D^2 law was observed [25]. Through a simple theoretical treatment we show how absorption of IR light drives this evaporation regime and leads to the observed scaling. After the droplet shrinks to a radius of 2–5 μm, we observe a turnover back to an accelerated shrinking rate with similar dynamics to the D^2 law.

Our findings provide new insights into the effect of low and high irradiative heating on droplet evaporation. This is relevant for applications ranging from combustion diagnostics and aerosol science to optically driven microfluidics and laser propulsion.

II. METHODS

A. Counter-propagating trap with IR heating

Figure 1 shows the counter-propagating optical trap in which water droplets are trapped and evaporate into the ambient air. The beam from a 532 nm continuous-wave laser (gem532) was expanded to 4.5 mm in diameter and split into two arms using a polarizing beam splitter. Each polarized beam was focused using a pair of 50 mm lenses in a counter-propagating arrangement, with beam waist at a focus of 3.7 ± 0.2 μm.

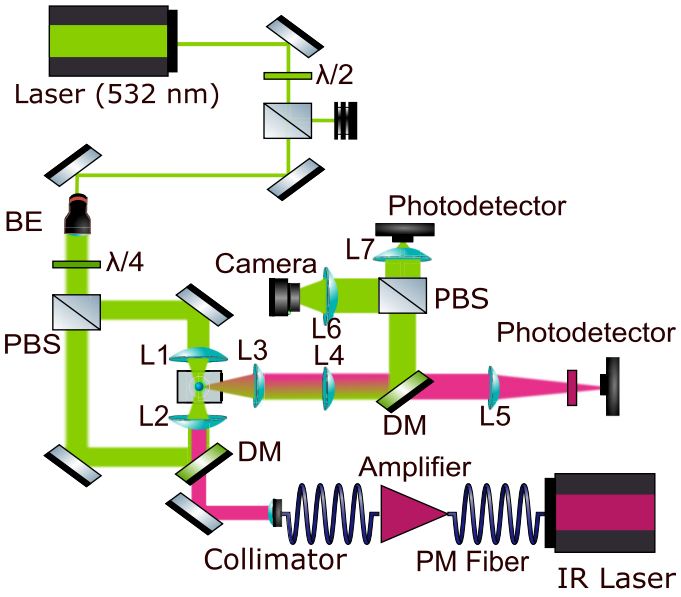


FIG. 1. Setup to measure the shrinking of individual micrometric water droplets under strong IR irradiation. A counter-propagating optical trap levitates the droplets between the lenses L1 and L2 (f = 50 mm for both lenses). The water droplets are heated with an IR laser beam parallel to the trapping beam and focused by L2.

This setup was similar to previous optical traps used to study droplet kinetics [20,22]. However, our setup can trap droplets with radii up to 10 μm and keep them trapped down to full evaporation. We achieved this using long focal-length lenses instead of microscope objectives in the counter-propagating trap, resulting in larger beam waists. In contrast to other studies where solutes such as salt and high-humidity environments are used to slow or even stop the evaporation [16,27], we instead let the droplets evaporate, allowing us to study the process without added solutes.

We used an ultrasonic nebulizer (MY-520A) to dispense a cloud of droplets into the chamber. The droplets fell randomly into the trap and merged up to a maximum droplet size defined by the optical trap. The continuous dispensing of water vapor resulted in a sustained high relative humidity (RH) inside the chamber of 98 ± 3% and an ambient temperature of 297 K.

To heat the droplets, we used an infrared (IR) laser (TLX1 C-Band Tunable Laser), set to a wavelength of 1550 ± 1 nm, amplified by an erbium-doped fiber amplifier (Thorlabs EDFA100P) as shown in Fig. 1. The fiber output was collimated to a beam diameter of 1.6 mm. The IR beam was focused by L2, resulting in a beam waist of 30.3 ± 0.2 μm. We scanned the power of the IR laser from 0 to 140 mW in steps of 10 mW. Importantly, the beam waist was always larger than the droplet radii under study, meaning that the droplets always received homogeneous laser heating.

B. Measuring the shrinking rate using the Fano comb structure

Spherical droplets can become resonance cavities for light. This happens when the light that evanescently couples into the droplet reflects around the inner water-air interface through total internal reflection. When the optical path is a multiple of the wavelength inside the material, constructive interference occurs and the droplet shines brighter. These are called whispering-gallery modes (WGM) and result in the droplet twinkling as it evaporates. Figure 2(a) shows the 90° scattering intensity of 532 nm light by a water droplet with a refractive index of $\bar{n} = 1.3355 + 2.6544 \times 10^{-9}i$ [28]. The scattering shows a Fano comb structure, named so because of the asymmetric Fano profile of the resonances on the far right side of the combs [29].

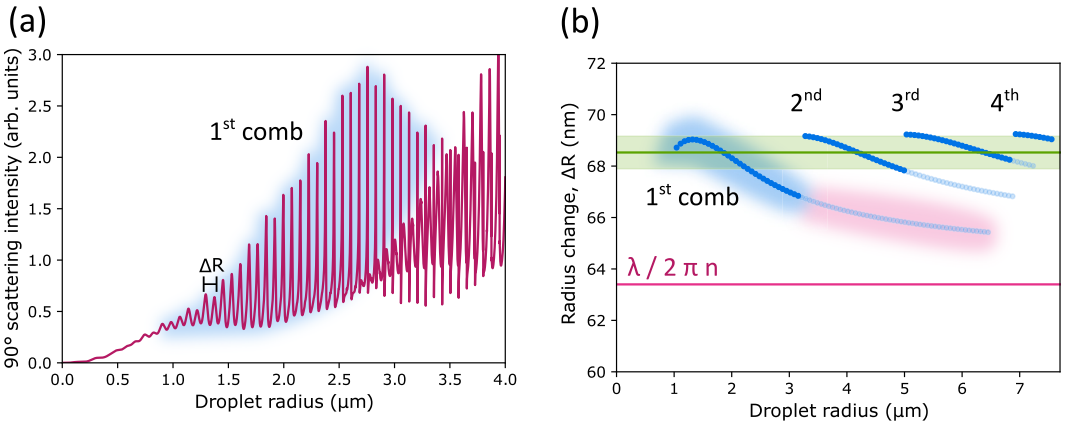


FIG. 2. We use the radius change of a droplet between consecutive resonances in the Fano comb pattern to measure the shrinking rate. (a) A simulation of the Fano comb spectrum at 532 nm scattered by a water droplet as it evaporates. The part of the spectrum where resonances in the first comb dominate is highlighted in blue. (b) A common approximation states that resonances occur every $\Delta R = \lambda/2\pi n$, plotted in magenta. The radius change between resonances calculated from the simulation is plotted in blue for the first four combs. The average radius change $\Delta R = 68.5 \pm 0.6$ nm is plotted with a horizontal green line with green shading representing one standard deviation. The radius changes from the dominating resonances in the first comb are highlighted in blue, while the radius changes from resonances hidden underneath the next comb are highlighted in magenta. We only use the dominating resonances in this work.

A common approximation is that resonances occur when the optical path of the light rotating around the circumference of the droplet, C, equals a multiple of the wavelength inside the material. Hence, resonances occur every time $C = m\lambda/n$ where m is an integer, λ is the wavelength, and n is the refractance. This approximate change in radius ΔR between resonances is plotted with a magenta horizontal line in Fig. 2(b). However, the exact radius change between resonances is plotted in blue in Fig. 2(b), showing that the approximation slightly underestimates the radius change. The dark blue line (highlighted in blue for the first comb) marks the radius changes between resonances of a comb that rises above any other comb, i.e., dominant resonances. The transparent line (highlighted in magenta) marks resonances that fall below those of the next comb. We find that radius change between dominant resonances is approximately constant with an average of $\Delta R = 68.5 \pm 0.6$ nm, plotted with a green line in Fig. 2(b).

In our experiments, we record time series of light scattered by evaporating droplets. To measure the shrinking rate, we assume the radius change between resonances to be constant and then measure the period between resonances Δt. Then, the shrinking rate is

$$\frac{dR}{dt} = \frac{\Delta R}{\Delta t}. \tag{1}$$

To be able to measure the resonances accurately, the levitating droplets in the trap have to be spherical. We characterize the sphericity through the Bond number

$$Bo = \frac{\Delta\rho\, g R^2}{\sigma},$$

where $\Delta\rho$ is the density difference between the droplet and surrounding medium, g is the gravitational acceleration, R is the droplet radius, and σ is the surface tension. Using the values stated in the Supplemental Material [30] (including Ref. [28]), the resulting Bond number is $Bo \sim 10^{-7} - 10^{-5}$, indicating that the surface tension dominates and the gravitational deformation is negligible. Therefore, the Mie solution to the droplet's scattering applies.

C. Fano combs vs the far-field scattering to measure shrinking rates

Several studies use a recording of the far-field light scattering (also called phase function) of the droplets to measure their size as they evaporate [15,22,27]. This has several advantages over using the Fano combs. To name a few, the sample rate is constant and depends on the frame rate of the camera, it measures the absolute size, and it is a well-established technique. Both techniques also share disadvantages, including the necessity of knowing *a priori* the refractive index. A comparison between these two methods can be found in Ref. [31].

However, the Mie resonance technique used in this work has other advantages. Most importantly, for small droplets, the far-field scattering can become so large that very few, if any, fringes are visible. This depends on the numerical aperture (NA) of the lens collecting the scattering of the droplets. Therefore, for applications where the light cannot be collected at short range with high NA, the Mie resonances technique provides access to measurements of small droplets with radii below 5 μm.

Secondly, it only requires a photodiode instead of a camera. This, on top of reducing the cost of the experiment, results in a measurement made up of a one-dimensional time series instead of a video, increasing the accessible sampling rate. Using the resonances, we achieved a maximum sampling rate of 1400 sps, which, although reachable with a high-speed camera, is two orders of magnitude faster than a normal 30 fps camera and has a much lower memory cost.

III. EXPERIMENTAL RESULTS

We dispensed a cloud of nebulized water droplets at room temperature into the trapping chamber. One or several of them fall into the laser trap and coalesce into the largest droplet the trap can sustain, i.e, $R \simeq 10\,\mu$m. Fano comb spectra were recorded for both the 532 nm and IR light scattering from the droplet. The spectrum at a wavelength of 532 nm was used to calculate the shrinking rate dR/dt. For the experiments regarding infrared (IR) irradiation, the droplets were trapped without IR irradiation first, and it was subsequently turned on to measure the shrinking.

A. Accelerated shrinking regime under low irradiative heating

We first measured the shrinking of droplets in the laser trap without IR irradiation. The absorbance of water at 532 nm is low, so we expect only a small influence of the 532 nm laser on the evaporation dynamics. The results presented here describe the evaporation of droplets under low irradiative heating in terms of the shrinkage rate.

Figure 3(a) shows an example of the twinkling of a water droplet as it evaporates. This light scattering forms a Fano comb pattern, where the dominating resonances are marked with green dots. We use the period between resonances to measure the radius of 10 separate droplets, shown in Fig. 3(b). The shrinking rate for these droplets is shown in Fig. 3(c) in a log-log scale. The linearity of the data shows that the evaporation of the droplets under these circumstances follows a power-law behavior. Note that the x axis represents the time before evaporation ends, $\tau = t_f - t$.

The blue line in Fig. 3(c), results from fitting the shrinking rate of all droplets using

$$\frac{dR}{d\tau} \propto \tau^{\beta}. \tag{2}$$

The measured exponent β at different trapping powers is plotted in Fig. 4. We find that β decreases linearly with respect to the trapping power, which is proportional to the laser irradiation. Extrapolating to 0 mW laser power we find that $\beta \to -0.5$. Note that the extrapolation is necessary since it is not possible to optically trap droplets in the absence of laser power.

It is relevant to note here the sign of the shrinking rate and its exponent. The shrinking rate appears positive as a function of τ. When written as a function of t, the change from $d\tau$ to dt carries a negative sign, resulting in a negative shrinking rate, as expected. To keep the time direction

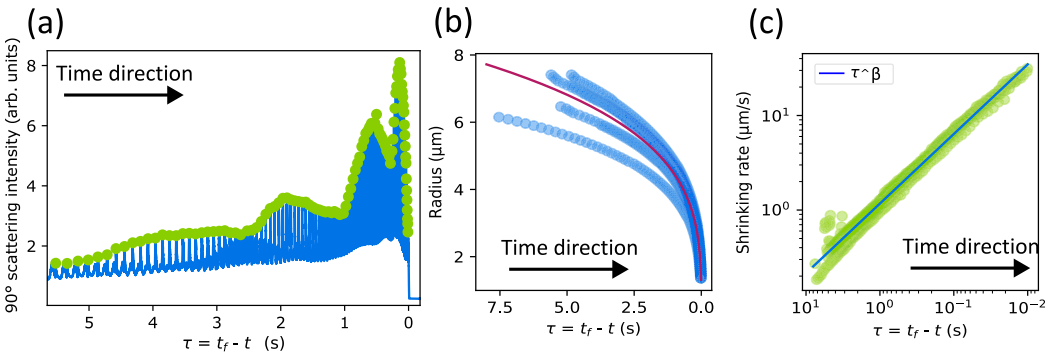


FIG. 3. Measuring the shrinking rate of levitating droplets in a laser trap without IR heating. The 523-nm trapping laser power was of 1 W. (a) Fano combs in the 90° light scattering of one representative evaporating water droplet. The green dots mark the resonances used to calculate the shrinking rate following the method described in Sec. II B. (b) Radii of ten separate droplets as they evaporate. The magenta line shows the average shrinking rate of the droplets using the power law in Eq. (2). (c) The shrinking rates dR/dt of ten separate water droplets in a laser trap (green dots). The data follows a power law with the obtained exponent of $\beta = -0.74 \pm 0.02$. Note: The x axis is inverted to keep the time direction towards the right. Because of this choice, negative exponents appear to have a positive slope and vice versa.

towards the right, we have inverted the x axis for all instances of τ. This causes negative exponents to appear positive, and vice versa.

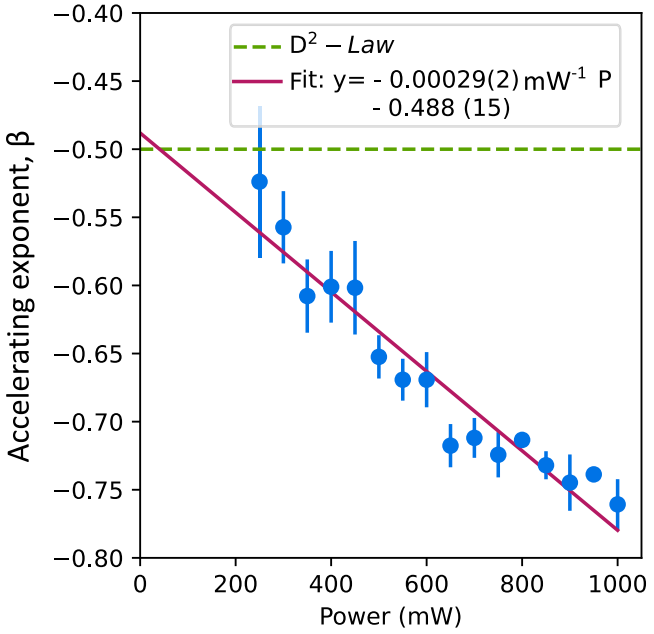


FIG. 4. The shrinking rate of optically levitated droplets (blue dots) tends towards the D^2 law (dashed green line) for decreasing trapping-laser power. The y axis shows the exponent of the power law [Eq. (2)] used to fit the data in Fig. 3(c), and the x axis shows the power of the trapping laser. As the trapping power increases, the increase in irradiative heating makes the exponent decrease linearly.

In the absence of irradiation, we expect that a stagnant droplet in relatively stationary surrounding air evaporates by solvent diffusion, that is driven by a concentration gradient of the solvent molecules in the air. For such a situation, the mass transfer into the air is described by the well-known D^2 law [24]

$$-\dot{m}(t) = 4\pi R(t) D_0 \Delta c, \tag{3}$$

where D_0 is the diffusion coefficient of the evaporating solvent in air and $\Delta c = c_i - c_\infty$ is the difference between the saturation concentration of the solvent at the droplet-air interface and the environment far away from the droplet. More complex formulations of the D^2 law (see, for instance, Ref. [32]) follow a similar scaling $\dot{m} \sim -R$. Rewriting and integrating the D^2 law leads to

$$R^2(t) = R_0^2 - K't, \tag{4}$$

with K' including all constant terms. When droplet disappears at t_f we have $R(t_f) = 0$ and thus $K't_f = R_0^2$ and $R^2(t) = K't_f - K't$. Combining this expression with $\tau = t_f - t$, we find

$$R^2(\tau) = K'\tau. \tag{5}$$

Therefore, we find that the time dependence of the radius is $R(\tau) \sim \tau^{1/2}$, and the shrinking rate is $\frac{dR}{d\tau} \sim \tau^{-1/2}$ and $\frac{dR}{d\tau} \sim R^{-1}$, which we observed as the no-irradiation limit (i.e., Power $\to$ 0) in Fig. 4.

Furthermore, the data in Fig. 4 shows that the small irradiative heating from the optical trap is already sufficient to decrease β in Eq. (2) compared to the D^2 law. In Sec. III C we show using a scaling argument that the irradiative contribution to the shrinking dynamics can be reasonably expected with our experimental settings. The negative exponent β means that the shrinking rate accelerates faster as the droplets evaporate. From here on, we will refer to this behavior as *accelerated shrinking*.

The shrinking rate could potentially further accelerate when considering the Kelvin effect, where the curvature of a droplet affects the vapor pressure of the species. However, under our experimental conditions, we find that for a 1 μm droplet, the vapor pressure increases by about 1%, as shown in the Supplemental Material [30], which is too small to be observed in our experiments.

B. Decelerated shrinking regime under high irradiative heating

For IR laser light the absorbance is almost 5 orders of magnitude higher compared to 532 nm. This strong irradiative heating results in different evaporation dynamics compared to what we showed in the previous section.

Figure 5 shows a typical evaporation process for a levitated droplet under strong irradiative heating. Figure 5(a) shows log-log plots of the shrinking rate as a function of time calculated from a Fano comb spectrum. The shrinking rate is used to calculate the radius as a function of time, plotted in linear scale in Fig. 5(b). Finally, (a) and (b) are used to plot the shrinking rate as a function of radius on a log-log scale in Fig. 5(c).

In the initial stage of the evaporation we find that the shrinking rate decreases as a function of time and radius, opposite to the behavior described by the D^2 law. We call this *decelerated shrinking*. Then we observe a turnover where, once the droplets shrink below a certain radius, we again observe an accelerated shrinking. We further observe that, even though the shrinking decelerates, the absolute value of the shrinking rate is much higher for a droplet under irradiative heating than without it. Comparing Fig. 3(c) with Fig. 5(c), the shrinking rate for a 10-μm radius droplet is almost two orders of magnitude higher under irradiative heating than it is in the absence of it.

We can capture the full shrinking profile in Fig. 5(c) using a sum of two power laws

$$\frac{dR}{d\tau} = A_2 R^\gamma + B_2 R^\delta . \tag{6}$$

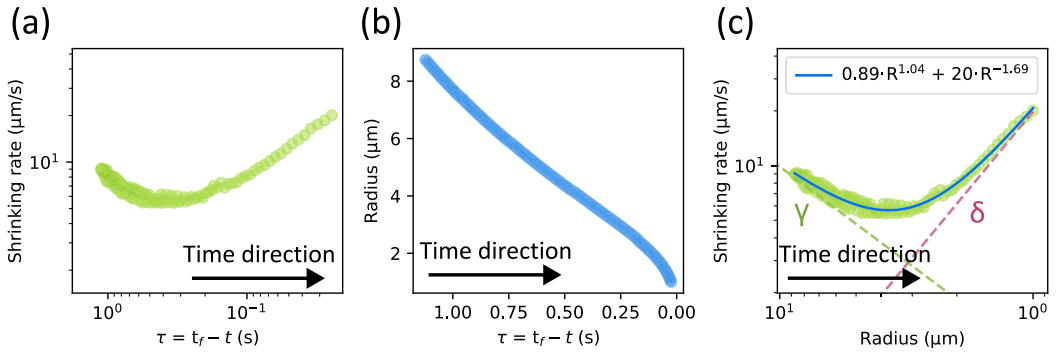


FIG. 5. The shrinking of droplets under high levels of irradiative heating decelerates at first. Beyond a certain size, the shrinking undergoes a turnover and returns to an accelerating regime. This figure shows one representative evaporation event of a water droplet in a 532 nm laser trap at 1 W and irradiated with a 130 mW IR beam. (a) Shrinking rate of one droplet as a function of time in log-log scale. (b) Radius of the droplet as a function of time. (c) Shrinking rate of the droplet as a function of radius in log-log scale. The blue line represents a fit using Eq. (6). The green and magenta dashed lines represent the left and right terms of the equation, respectively. The exponent values are $\gamma = 1.04 \pm 0.05$ and $\delta = -1.69 \pm 0.05$.

The dashed lines show the individual terms of the equations, with green representing the first term with exponent γ and magenta the second term with exponents δ.

We note that Eq. (6) is an empirical expression using a linear combination of two limiting regimes, which we expect are laser-induced and diffusive shrinking. As this phenomenological expression well describes our experimental data, it appears that laser-induced and diffusive dynamics contribute over overlapping radius windows, leading to the turnover observed in the intermediate regime. Providing a detailed description of the physics in this intermediate regime is beyond the scope of this paper.

We consistently find that the value of γ representing the slope of the decelerated shrinking regime is approximately equal to 1, as shown in Fig. 6. This means that the shrinking rate decreases linearly with droplet radius for large droplets under irradiative heating. Furthermore, Fig. 6 shows that this exponent is independent of laser power, averaging to a value of 1.03 ± 0.21 over a range of IR power from 30 mW to 140 mW. Finally, we note that the exponent in the accelerated shrinking regime δ is reduced compared to the expected value in purely diffusive dynamics, $\delta = -1$, which agrees with our previous observations under slight VIS irradiation in Fig. 4.

C. A theoretical model for evaporation under strong irradiation

Next, we present a theoretical analysis for decelerated shrinking in the limit where $\gamma \to 1$, as observed when using the IR laser for the larger size ranges in Fig. 5. The model relies on the following assumptions: (i) The droplet under strong irradiative heating reaches a steady state with constant temperature where all the heat from the lasers is lost through evaporation, as shown in Ref. [25], where the temperature reaches an approximately constant level. (ii) The irradiative heating is so strong that this dominates over the other sources of heat, which we assume are are negligible. (iii) The heat loss through evaporation is dominant while the convective and radiative heat loss is negligible. (iv) The droplet maintains a spherical shape.

With these assumptions, the heat balance can be written as

$$\dot{Q}_{\text{abs,trap}} + \dot{Q}_{\text{abs,IR}} = \dot{Q}_{\text{evap}}, \tag{7}$$

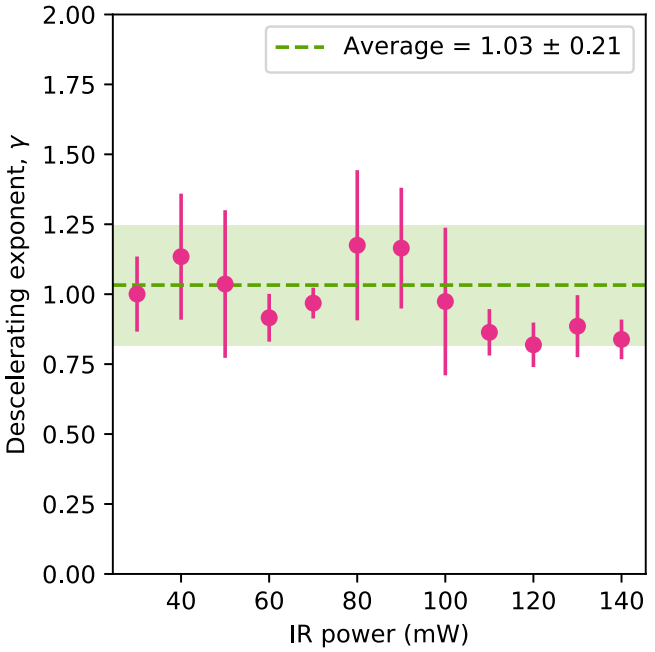


FIG. 6. The exponent of the power law in the decelerating, irradiation regime is close to 1 for varying levels of IR irradiation. Each magenta dot shows the average value of the γ exponent in Eq. (6) for up to ten different droplets evaporating at a constant power of IR irradiation. The power of the 532 nm trapping laser was constant at 1 W.

where $\dot{Q}_{\text{abs,trap}}$ and $\dot{Q}_{\text{abs,IR}}$ are the heat absorption rates from the trapping and IR lasers. The heat loss due to evaporation is

$$\dot{Q}_{\text{evap}} = \dot{m}L, \tag{8}$$

where L is the latent heat of vaporization and $\dot{m}$ the mass evaporaiton rate. $\dot{m}$ can be related to the radius change as

$$\dot{m} = -\rho_l \frac{dV}{dt} = -\rho_l \cdot 4\pi R^2 \frac{dR}{dt}. \tag{9}$$

Solving for the shrinking rate, we obtain

$$\frac{dR}{dt} = -\frac{\dot{Q}_{\text{abs,trap}} + \dot{Q}_{\text{abs,IR}}}{4\pi \rho_l L R^2}. \tag{10}$$

For both the optical trap and the IR laser, the heat absorption rate $\dot{Q}_{\text{abs}}$ of the droplet is given by

$$\dot{Q}_{\text{abs}} = q_{\text{abs}} \cdot I_{\text{laser}} \cdot A_{\text{droplet}}, \tag{11}$$

where q_{abs} is the Mie absorption efficiency, I_{laser} is the irradiation of the laser and A_{droplet} is the droplet cross-sectional area. Using $I_{\text{laser}} = P_{\text{laser}}/A_{\text{beam}}$, where P_{laser} is the laser power, A_{beam} is the cross-sectional area at the waist of the beam, and $A_{\text{droplet}} = 4\pi R^2$, Eq. (11) can be further expressed as

$$\dot{Q}_{\text{abs}} = q_{\text{abs}} \cdot \frac{P_{\text{laser}}}{A_{\text{beam}}} \cdot \pi R^2. \tag{12}$$

Here, q_{abs} represents the absorption efficiency of light by the droplet. In the geometrical optics approximation, this efficiency is proportional to the droplet radius $q_{\text{abs}} = \chi R$, as detailed in Ref. [33].

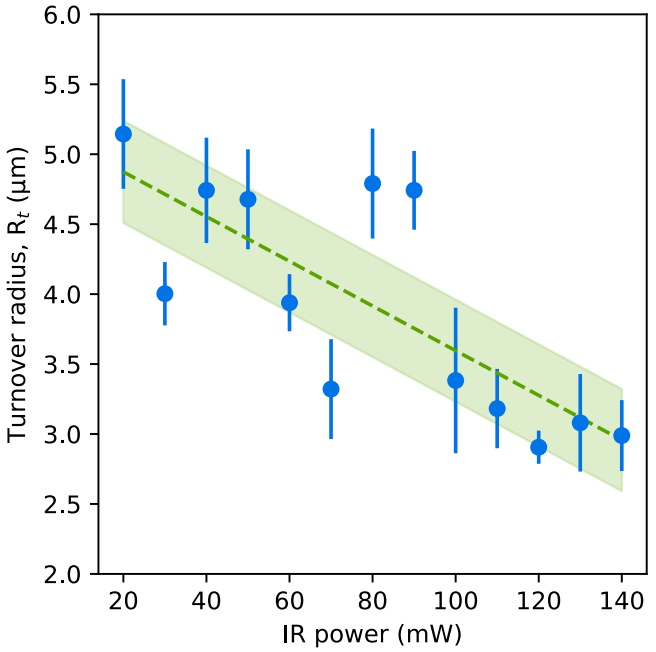


FIG. 7. The turnover radius where the shrinking of the droplets transitions from the decelerating regime to the accelerating regime decreases at increasing powers of IR irradiation. Applying a linear fit (green dashed line), we find that the turnover radius decreases by 0.018 ± 0.004 μm/mW of IR irradiation power. The trapping power was constant at 1 W. The blue dots show an average of the radii at which the minimum shrinking rate occurs, i.e., the minimum value of blue curve in Fig. 5(c).

In the case of small droplets, the geometrical optics approximation and the exact Mie solution are in good agreement [33], except for the effects of Mie resonances, which are explored in Sec. III E. Here, $\chi = (4/3)(\alpha/(n_{\text{wter}}/n_{\text{air}}))[(n_{\text{wter}}/n_{\text{air}})^3 - ((n_{\text{wter}}/n_{\text{air}})^2 - 1)^{3/2}]$ is a constant dependent on the refractive indices, n_i, and the absorption coefficient of the droplet, α [33].

Then, by substituting Eq. (12) into Eq. (10) we obtain the final result

$$\frac{dR}{dt} = -\frac{R(P_{\text{trap}}\chi_{\text{trap}} + P_{IR}\chi_{IR})}{4A_{\text{beam}}\rho_l L}. \tag{13}$$

Equation (13) shows the proportionality $dR/dt \sim R^1$, which we observed in Fig. 6. Therefore, we propose that the strong irradiative heating, in this case provided by the absorption of the IR beam, dominates the evaporation dynamics in our experiments in the early-times regime where $\gamma \to 1$.

Equation (13) also allows us to estimate the relative contribution of the heating from the visible and IR laser beams to the shrinking rate. For the 532 nm beam ($\alpha \sim 0.0345$/m, $n_{\text{wter}}/n_{\text{air}} = 1.335$, $P_{\text{trap}} = 1$ W, $w_b = 3.7$ μm) we calculate for a 10-μm droplet the shrinking rate $\frac{dR}{dt} \sim -\frac{RP_{\text{trap}}\chi_{\text{trap}}}{4A_{\text{beam}}\rho_l L} \approx 1.5$ μm/s. For comparison, in the IR laser ($\alpha \sim 799.59$/m, $n_{\text{wter}}/n_{\text{air}} = 1.316$, $P_{IR} = 130$ mW, $w_b = 30.3$ μm) we find $\frac{dR}{dt} \sim -\frac{RP_{IR}\chi_{IR}}{4A_{\text{beam}}} \approx 66$ μm/s, which is about 40 times higher and explains why we only observe the decelerated shrinking regime when using the IR laser.

We note that this calculation overestimates the absolute value of the shrinking rate in our experiments, as scattering and absorption by small water droplets in the beamline reduces the total amount of laser power that reaches the droplet in the trap. Additionally, the droplet will not be exactly at the focal point, which increases A_{beam} and thus reduces the power density.

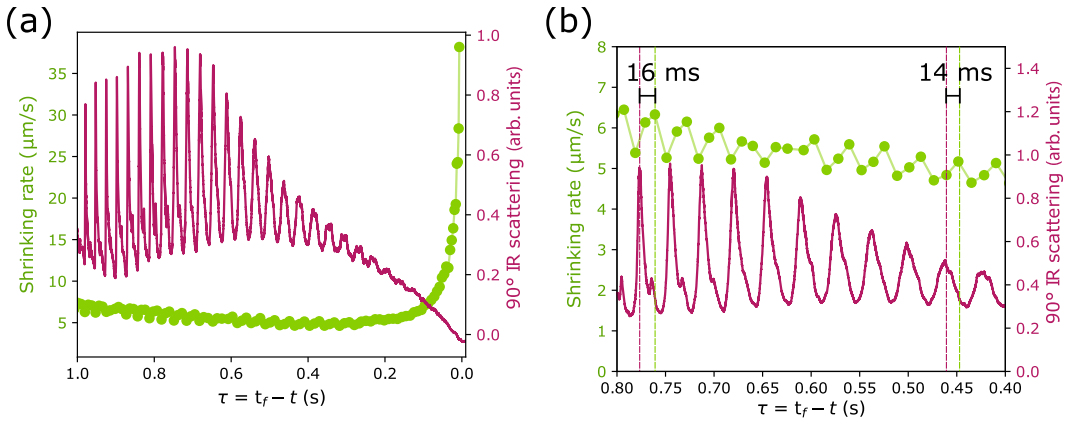


FIG. 8. Fast increase in the shrinking rate of a droplet following a Mie resonance. (a) Mie combs in the IR scattering of the droplet (magenta, right y axis) and the shrinking rate (green dots, left y axis). (b) Zoomed-in plot of the shrinking rate showing the increases caused by the increased absorption because of the Mie resonances. The power of the IR beam was 130 mW and that of the trapping laser was 1 W.

D. Turnover from an irradiation-driven, decelerated shrinking back to an accelerated shrinking regime

At a specific radius and a given IR irradiation power, a droplet has a minimum shrinking rate where it transitions from a decelerating to an accelerating regime. We call this radius the turnover radius R_t. Figure 7 shows the average turnover radius for droplets shrinking under increasing IR irradiation power. We find that R_t decreases from about 5 μm at medium irradiative heating down to 3 μm at high irradiative heating.

E. Heating during a WGM resonance

Additionally, we measured the IR scattering, shown in magenta in Fig. 8(a), simultaneously with the measurement of the 532 nm laser used to calculate the shrinking rate, shown in green dots. The Mie Fano-comb spectrum in the IR has a similar profile as for 532 nm, but since the wavelength is longer we only see one comb. Zooming in to a 400 ms segment of Fig. 8(a) shows that the shrinking rate follows a periodic oscillation from fast to slow in correlation with the IR resonances. Since we use the resonances at 532 nm to measure the shrinking rate and the IR wavelength is about three times larger, we obtain three shrinking-rate measurements per IR resonance.

The increased heat absorbance during Mie resonances is well known [33]. However, we can use this fact showcased in Fig. 8(b) to illustrate how the shrinking rate can adapt fast to changes in irradiation. We observe increases of 10–15% in shrinking rate with a delay of 14–16 ms between the Mie resonance and the peak shrinking speed.

IV. CONCLUSION

This work showcases the effects of weak and strong irradiative heating on the evaporation of levitating water droplets with radii below 10 μm. Under weak irradiative heating, we find that the shrinking rate accelerates following a power law similar to the classical D^2 law. However, under strong irradiative heating we find a decelerating regime where the irradiation drives the evaporation dynamics, which is very different from the D^2 law. Between these two regimes we observe a turnover in the evaporation dynamics at radii of 3–5 μm. The counter-propagating optical trap and the Mie resonance technique we used allowed us to measure the shrinking rates of the droplets accurately and with a high sampling rate.

Our results provide an overview of the effects at varying levels of irradiation. Furthermore, our theoretical model suggests that evaporation in the limit of high irradiation is dominated by Mie absorption, which is important for understanding evaporation dynamics in many applications in nature and industry. Such applications can range from low irradiative heating of aerosol droplets in the atmosphere to the high irradiative heating of droplets illuminated by flames in internal combustion engines.

ACKNOWLEDGMENTS

Financial support from the Swedish Research Council (Grants No. 2019-02376_VR and No. 2020-03505_VR) is acknowledged. J.T.M. acknowledges support from The Märta and Eric Holmberg Endowment and Stiftelsen Lars Hiertas Minne. M.H. was funded by the University of Edinburgh. J.S. acknowledges support from Erasmus+ program of the European Union. We thank Ingemar Magnusson, Simon Titmuss, and Wilson Poon for discussions regarding the interpretation of our results.

J.T.M. conceptualized the experiment. J.S. and J.T.M. built the experimental setup, performed the experiments, and analyzed the data. J.S., J.T.M., and M.H. wrote the first draft of the manuscript. J.S. and M.H. contributed to the interpretation of the data and the theoretical background. D.H., D.D., and J.T.M. supervised the project. All authors contributed to the final version of the manuscript.

DATA AVAILABILITY

The data that support the findings of this article are openly available [34], embargo periods may apply.

[1] R. Vehring, Pharmaceutical particle engineering via spray drying, Pharm. Res. **25**, 999 (2008).

[2] V. Dugas, J. Broutin, and E. Souteyrand, Droplet evaporation study applied to DNA chip manufacturing, Langmuir **21**, 9130 (2005).

[3] S. C. Ray, Safiullah, S. Naito, M. Andersson, K. Nishida, and Y. Ogata, Evaluation of vaporizing diesel spray with high-speed laser absorption scattering technique for measuring vapor and liquid phase concentration distributions, Fuels **4**, 75 (2023).

[4] S. Kotake and T. Okazaki, Evaporation and combustion of a fuel droplet, Int. J. Heat Mass Transf. **12**, 595 (1969).

[5] K. Sezen and A. Gungor, Water droplet evaporation in atmospheric air stream, Phys. Fluids **35**, 017122 (2023).

[6] K. Sefiane, On the formation of regular patterns from drying droplets and their potential use for bio-medical applications, J. Bionic Eng. **7**, S82 (2010).

[7] B. Wang, Y. Xuan, and X. Han, Analysis on roles of thermal radiation to evaporation and combustion of fuel droplets, Int. J. Therm. Sci. **191**, 108306 (2023).

[8] G. R. Leung, S. M. Saleeby, G. A. Sokolowsky, S. W. Freeman, and S. C. van den Heever, Aerosol–cloud impacts on aerosol detrainment and rainout in shallow maritime tropical clouds, Atmos. Chem. Phys. **23**, 5263 (2023).

[9] M. K. Tripathi and K. C. Sahu, Evaporating falling drop, Procedia IUTAM **15**, 201 (2015).

[10] L. Jiao, R. Chen, X. Zhu, and Q. Liao, Ir laser caused droplet evaporation on the hydrophobic surface, Int. J. Heat Mass Transf. **94**, 180 (2016).

[11] Y. Jin, W. Xu, H. Zhang, R. Li, J. Sun, S. Yang, M. Liu, H. Mao, and Z. Wang, Electrostatic tweezer for droplet manipulation, Proc. Natl. Acad. Sci. USA **119**, e2105459119 (2022).

[12] B . Ali Al Zaitone and C. Tropea, Evaporation of pure liquid droplets: Comparison of droplet evaporation in an acoustic field versus glass-filament, Chem. Eng. Sci. **66**, 3914 (2011).

[13] D. Jakubczyk, M. Zientara, G. Derkachov, K. Kolwas, and M. Kolwas, Investigation of the evolution of charged water droplets in the electrodynamic trap, in *Tenth Joint International Symposium on Atmospheric and Ocean Optics/Atmospheric Physics. Part II: Laser Sensing and Atmospheric Physics* (SPIE, 2004), Vol. 5397, pp. 23–33.
[14] K.-Y. Li, H. Tu, and A. K. Ray, Charge limits on droplets during evaporation, Langmuir **21**, 3786 (2005).
[15] Y.-y. Su, R. E. H. Miles, Z.-m. Li, J. P. Reid, and J. Xu, The evaporation kinetics of pure water droplets at varying drying rates and the use of evaporation rates to infer the gas phase relative humidity, Phys. Chem. Chem. Phys. **20**, 23453 (2018).
[16] A. Haddrell, G. Rovelli, D. Lewis, T. Church, and J. Reid, Identifying time-dependent changes in the morphology of an individual aerosol particle from its light scattering pattern, Aerosol Sci. Technol. **53**, 1334 (2019).
[17] G. Barrios and R. Rechtman, Dynamics of an acoustically levitated particle using the lattice Boltzmann method, J. Fluid Mech. **596**, 191 (2008).
[18] R. Bowman, A. Jesacher, G. Thalhammer, G. Gibson, M. Ritsch-Marte, and M. Padgett, Position clamping in a holographic counterpropagating optical trap, Opt. Express **19**, 9908 (2011).
[19] R. Pastel and A. Struthers, Measuring evaporation rates of laser-trapped droplets by use of fluorescent morphology-dependent resonances, Appl. Opt. **40**, 2510 (2001).
[20] A. Rafferty and T. C. Preston, Measuring the size and complex refractive index of an aqueous aerosol particle using electromagnetic heating and cavity-enhanced Raman scattering, Phys. Chem. Chem. Phys. **20**, 17038 (2018).
[21] R. E. H. Miles, J. S. Walker, D. R. Burnham, and J. P. Reid, Retrieval of the complex refractive index of aerosol droplets from optical tweezers measurements, Phys. Chem. Chem. Phys. **14**, 3037 (2012).
[22] M. E. Diveky, M. J. Gleichweit, S. Roy, and R. Signorell, Shining new light on the kinetics of water uptake by organic aerosol particles, J. Phys. Chem. A **125**, 3528 (2021).
[23] A. Rafferty and T. C. Preston, Trapping positions in a dual-beam optical trap, J. Appl. Phys. **130**, 183105 (2021).
[24] I. Langmuir, The evaporation of small spheres, Phys. Rev. **12**, 368 (1918).
[25] S. Pokharel, A. Tropina, and M. Shneider, Numerical modeling of laser heating and evaporation of a single droplet, Energies **16**, 388 (2022).
[26] D. Zhang, M. Tu, Y. Yuan, and W. Han, Thermal radiative transfer characteristics of a single water droplet, Int. J. Heat Mass Transf. **219**, 124824 (2024).
[27] F. K. A. Gregson, J. F. Robinson, R. E. H. Miles, C. P. Royall, and J. P. Reid, Drying kinetics of salt solution droplets: Water evaporation rates and crystallization, J. Phys. Chem. B **123**, 266 (2019).
[28] S. Kedenburg, M. Vieweg, T. Gissibl, and H. Giessen, Linear refractive index and absorption measurements of nonlinear optical liquids in the visible and near-infrared spectral region, Opt. Mater. Express **2**, 1588 (2012).
[29] J. T. Marmolejo, A. Canales, D. Hanstorp, and R. Méndez-Fragoso, Fano combs in the directional Mie scattering of a water droplet, Phys. Rev. Lett. **130**, 043804 (2023).
[30] See Supplemental Material at http://link.aps.org/supplemental/10.1103/92w3-x9q4 for a list of constants and parameters, some additional equations, and an estimation of the Kelvin effect.
[31] D. C. Taflin, S. H. Zhang, T. Allen, and E. J. Davis, Measurement of droplet interfacial phenomena by light-scattering techniques, AIChE J. **34**, 1310 (1988).
[32] J. Kukkonen, T. Vesala, and M. Kulmala, The interdependence of evaporation and settling for airborne freely falling droplets, J. Aerosol Sci. **20**, 749 (1989).
[33] C. F. Bohren and D. R. Huffman, *Absorption and Scattering of Light by Small Particles* (Wiley-VCH Verlag GmbH, Weinheim, Germany, 2008).
[34] J. T. Marmolejo, D. Hanstorp, J. Shah, M. Huisman, and D. Deshmukh, Raw data for "Irradiation-driven evaporation of micro droplets in an optical trap", Dataset (2024), https://doi.org/10.6084/m9.figshare.28028663.v1.